Experimental Study of Compressional Hydromagnetic Waves

D. G. SWANSON, R. W. GOULD, AND R. H. HERTEL
California Institute of Technology, Pasadena, California
(Received 5 August 1963)

An experiment is described in which a compressional hydromagnetic wave is observed in a hydrogen plasma-filled waveguide. The theory of a cool, partially ionized, resistive plasma in a magnetic field is described briefly and expressions are derived for the dispersion relation and transfer function which include both the propagation and attenuation constants as a function of frequency. Measurements of the cutoff frequency are presented, which verify its linear dependence on the magnetic field, and they show good agreement with theory on the variation with the ion mass density. The impulse response of the plasma is studied, transformed into the frequency domain, and quantitative comparisons are made with the theoretical transfer function to determine the degree of ionization, the resistivity, and the ion–neutral collision frequency.

Results indicate that the degree of ionization varies over a range from 75% to 45% when the initial density varies from 1.3×10^{21} to 1.4×10^{22} atoms/m^3. The measured resistivity appears to increase with the magnetic field, with the mean value corresponding to a temperature of the order of 5×10^3 °K. The average value of the product of the charge exchange cross section and the neutral thermal speed is found to be approximately $(5.5 \pm 1.3) \times 10^{-15}$ m^3/sec.

I. INTRODUCTION

HYDROMAGNETIC waves, which were first described by Alfvén[1] in 1942, have been observed in recent years in gaseous plasmas.[2–4] All of the above experiments have studied the waveguide mode which has a resonance at the ion cyclotron frequency, whereas Newcomb[5] and others[6,7] have shown that two distinct modes will propagate in a hydromagnetic waveguide. One of these has no resonance at the ion cyclotron frequency but does have a low frequency cutoff. The experimental observation of this latter mode, which we call the compressional mode, was only recently reported by Hooke *et al.*,[8] the authors,[9] and by Jephcott.[10] This investigation is an extension of the work reported by the authors.

In this paper the theory of a three-fluid model for a cold plasma in a magnetic field is first developed and solutions for hydromagnetic waves in a plasma filled waveguide are obtained. An experiment on the compressional hydromagnetic wave is then described which uses the geometry of Fig. 1 to test the adequacy of the plasma model and to determine the plasma parameters. In the experiment we have developed a pulse technique which enables us to measure the dispersion relation from below cutoff to above the ion cyclotron frequency on a single shot, so uncertainties due to nonreproducibility have been avoided. This technique involves computing the Fourier transform of the response to an impulse excitation, and comparing the transform with a theoretical transfer function. Curve fitting is used in the comparison to determine the degree of ionization, the resistivity, and the ion–neutral collision frequency.

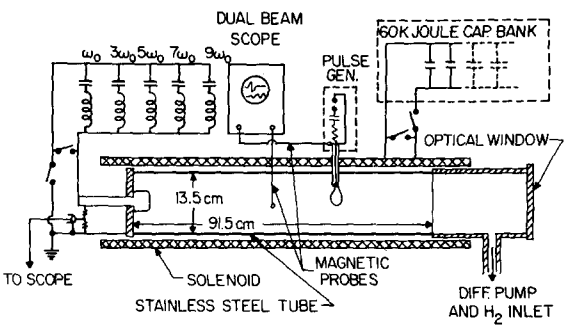

FIG. 1. Schematic diagram of experimental apparatus.

II. PLASMA MODEL

For a model of the plasma in a plasma filled waveguide we consider a cold three-fluid plasma which is uniform, neutral, axially magnetized, and composed of electrons, singly charged ions, and neutral atoms which interact with each other by electron–ion and ion–neutral collisions. We neglect the pressure or thermal effects since we assume that

[1] H. Alfvén, Ark. Mat., Astr. Fysik **29B**, 1 (1942).
[2] T. K. Allen, W. R. Baker, R. V. Pyle, and J. M. Wilcox, Phys. Rev. Letters **2**, 383 (1959); J. M. Wilcox, F. I. Boley, and A. W. DeSilva, Phys. Fluids **3**, 15 (1960).
[3] D. F. Jephcott, Nature **183**, 1652 (1959).
[4] T. H. Stix, Phys. Rev. **106**, 1146 (1957).
[5] W. A. Newcomb, *Magnetohydrodynamics* (Stanford University Press, Stanford, California, 1957), p. 109.
[6] R. Gajewski, Phys. Fluids **2**, 633 (1959).
[7] L. C. Woods, J. Fluid Mech. **13**, 570 (1962).
[8] W. M. Hooke, M. A. Rothman, P. Avivi, and J. Adam, Phys. Fluids **5**, 864 (1962).
[9] D. G. Swanson and R. W. Gould, Bull. Am. Phys. Soc. **8**, 152 (1963).
[10] D. F. Jephcott, Bull. Am. Phys. Soc. **8**, 152 (1963).

$p_m = B^2/2\mu_0 \gg nkT$, or that the Alfvén speed is much greater than the sound speed. We consider only small perturbations from the steady state and assume $e^{i\omega t}$ time dependence so that we may use the linearized second moments of the Boltzmann equations with the time derivatives replaced by $i\omega$. Hence we may write

$$i\omega n_e m_e \mathbf{v}_e = -n_e e(\mathbf{E} + \mathbf{v}_e \times \mathbf{B}_0) + \mathbf{P}^{ei}, \tag{1a}$$

$$i\omega n_i m_i \mathbf{v}_i = n_i e(\mathbf{E} + \mathbf{v}_i \times \mathbf{B}_0) + \mathbf{P}^{ie} + \mathbf{P}^{in}, \tag{1b}$$

$$i\omega n_n m_n \mathbf{v}_n = \mathbf{P}^{ni}, \tag{1c}$$

where the subscripts and superscripts e, i, and n refer to electrons, ions, and neutrals respectively, and the $\mathbf{P}^{ij}$ represent the momentum per unit volume per second transferred from the jth to the ith species of the plasma due to collisions.

To obtain an expression for $\mathbf{P}^{ni}$, we assume that the charge-exchange cross section is dominant for ion–neutral momentum transfer, and that the neutrals are comprised principally of atoms. A charge exchange collision is effectively head-on, since little momentum is actually exchanged, in which case the momentum gained by a neutral atom per collision is very nearly $m_n(\mathbf{v}_i - \mathbf{v}_n)$, since $m_i \approx m_n$. $\mathbf{P}^{ni}$ is then given by the product of this term and the neutral particle density times the collision frequency ν of a neutral with any ion. Hence we have

$$\mathbf{P}^{ni} = n_n m_n(\mathbf{v}_i - \mathbf{v}_n)\nu. \tag{2}$$

Using Eqs. (2) and (1c) we may solve for $\mathbf{v}_n$ in terms of $\mathbf{v}_i$ and then use this result again in (2) to obtain an expression for $\mathbf{P}^{ni}$ in terms of $\mathbf{v}_i$. Since $\mathbf{P}^{ij} = -\mathbf{P}^{ji}$, we may use this result in Eq. (1b), where, if we let $m_n = m_i$, we may write the result in the form

$$i\omega \mathbf{v}_i n_i m_i \left[1 + \frac{n_n}{n_i(1 + i\omega/\nu)}\right] = n_i e(\mathbf{E} + \mathbf{v}_i \times \mathbf{B}_0) + \mathbf{P}^{ie}. \tag{3}$$

This result may be interpreted as the equation of motion for a pseudo-ion with mass μ, where

$$\mu = m_i\left[1 + \frac{n_n}{n_i(1 + i\omega/\nu)}\right]. \tag{4}$$

If we consider the $\mathbf{P}^{ei}$ term to be proportional to the difference in average velocities of the ions and electrons, or to the current, and define the constant of proportionality by (where $n_i = n_e = n$)

$$\eta \mathbf{J} \equiv \frac{\mathbf{P}^{ei}}{ne} = -\frac{\mathbf{P}^{ie}}{ne}, \tag{5}$$

then η corresponds to the resistivity as given by Spitzer.[11] Using these expressions along with

$$\mathbf{J} = ne(\mathbf{v}_i - \mathbf{v}_e), \tag{6}$$

we may solve the coupled equations for $\mathbf{J}$ in terms of $\mathbf{E}$, and if we assume $\mathbf{B}_0$ is in the z direction, the result may be summarized by writing an effective conductivity tensor $\mathfrak{d}$

$$\begin{bmatrix} J_r \\ J_\theta \\ J_z \end{bmatrix} = \begin{bmatrix} \sigma_1 & i\sigma_2 & 0 \\ -i\sigma_2 & \sigma_1 & 0 \\ 0 & 0 & \sigma_3 \end{bmatrix} \begin{bmatrix} E_r \\ E_\theta \\ E_z \end{bmatrix} \tag{7}$$

where

$$\sigma_1 = \frac{\sigma_1' + \eta(\sigma_1'^2 - \sigma_2'^2)}{1 + 2\eta\sigma_1' + \eta^2(\sigma_1'^2 - \sigma_2'^2)}, \tag{8a}$$

$$\sigma_2 = \frac{\sigma_2'}{1 + 2\eta\sigma_1' + \eta^2(\sigma_1'^2 - \sigma_2'^2)}, \tag{8b}$$

$$\sigma_3 = \sigma_3'/(1 + \eta\sigma_3'), \tag{8c}$$

$$\sigma_1' = \left(\frac{\omega_p^2}{\omega_c^2 - \omega^2} + \frac{\Omega_p^2}{\Omega_c^2 - \omega^2}\right) i\omega\epsilon_0, \tag{9a}$$

$$\sigma_2' = \left(\frac{\omega_p^2\omega_c}{\omega_c^2 - \omega^2} - \frac{\Omega_p^2\Omega_c}{\Omega_c^2 - \omega^2}\right) i\epsilon_0, \tag{9b}$$

$$\sigma_3' = (\omega_p^2 + \Omega_p^2)\epsilon_0/i\omega, \tag{9c}$$

$$\omega_p^2 = ne^2/m_e\epsilon_0, \qquad \Omega_p^2 = ne^2/\mu\epsilon_0, \qquad \omega_c = eB_0/m_e, \qquad \Omega_c = eB_0/\mu. \tag{10}$$

We note that the effective conductivity tensor $\mathfrak{d}$ reduces to the $\mathfrak{d}'$ tensor when $\eta \to 0$, and that this tensor becomes the ordinary cold collisionless, two-fluid conductivity when $\nu \to 0$ so that the pseudo-ion mass μ reduces to the ordinary ion mass m_i.

We now wish to incorporate the current $\mathbf{J}$ in the Maxwell's equation such that

$$\nabla \times \mathbf{H} = \mathbf{J} + i\omega\epsilon_0\mathbf{E} \equiv i\omega\mathfrak{e}\cdot\mathbf{E}, \tag{11}$$

so we have

$$i\omega\mathfrak{e} = \mathfrak{d} + i\omega\epsilon_0\mathbf{1}, \tag{12}$$

and the effective dielectric tensor so defined contains all of the information about the plasma. Equation (11) is now to be solved along with

$$\nabla \times \mathbf{E} = -i\omega\mu_0\mathbf{H}, \tag{13}$$

with the conducting cylindrical waveguide boundary condition.

[11] L. Spitzer, Jr., *Physics of Fully Ionized Gases* (Interscience Publishers Inc., New York, 1957), p. 21.

III. DERIVATION OF DISPERSION RELATION

We restrict ourselves to circularly symmetric modes in the solution of Eqs. (11) and (13), although the general solution to these equations has been obtained.[12] We may assume the fields to vary as $e^{i(\omega t-kz)}$ since we are interested in propagation down the waveguide. Equations (11) and (13) may now be used to solve for the transverse components of the wave fields in terms of the longitudinal components and their derivatives, and finally a pair of coupled equations for H_z and E_z may be derived which are

$$\frac{ia}{r}\frac{\partial}{\partial r}\left(r\frac{\partial H_z}{\partial r}\right)+i\omega\mu_0 H_z+\frac{b}{r}\frac{\partial}{\partial r}\left(r\frac{\partial E_z}{\partial r}\right)=0 \tag{14a}$$

$$\frac{ic}{r}\frac{\partial}{\partial r}\left(r\frac{\partial E_z}{\partial r}\right)-i\omega\epsilon_3 E_z+\frac{b}{r}\frac{\partial}{\partial r}\left(r\frac{\partial E_z}{\partial r}\right)=0 \tag{14b}$$

where

$$a\equiv\frac{-\omega\mu_0\gamma_1}{\gamma_1^2-\gamma_2^2},\qquad b\equiv\frac{k\gamma_2}{\gamma_1^2-\gamma_2^2},$$
$$c\equiv\frac{\omega\epsilon_1\gamma_1+\omega\epsilon_2\gamma_2}{\gamma_1^2-\gamma_2^2}, \tag{15}$$

and

$$\gamma_1\equiv k^2-\omega^2\mu_0\epsilon_1,\qquad \gamma_2\equiv\omega^2\mu_0\epsilon_2.$$

To find a solution of these coupled equations we assume that $H_z=\phi$ and $E_z=\alpha\phi$ where α is a constant, thus obtaining

$$(ia+\alpha b)\frac{1}{r}\frac{\partial}{\partial r}\left(r\frac{\partial\phi}{\partial r}\right)+i\omega\mu_0\phi=0, \tag{16a}$$

$$(ic\alpha+b)\frac{1}{r}\frac{\partial}{\partial r}\left(r\frac{\partial\phi}{\partial r}\right)-i\omega\epsilon_3\alpha\phi=0. \tag{16b}$$

For a compatible, nontrivial solution the determinant of coefficients must vanish and this yields a quadratic equation for α. If we label the two solutions of this quadratic equation by α_1 and α_2 we have

$$H_z=\phi_1+\phi_2, \tag{17a}$$

$$E_z=\alpha_1\phi_1+\alpha_2\phi_2, \tag{17b}$$

where ϕ_1 and ϕ_2 are the solutions of the differential equations

$$\frac{1}{r}\frac{\partial}{\partial r}\left(r\frac{\partial\phi_1}{\partial r}\right)+\left(\frac{i\omega\mu_0}{ia+\alpha_1 b}\right)\phi_1=0, \tag{18a}$$

$$\frac{1}{r}\frac{\partial}{\partial r}\left(r\frac{\partial\phi_2}{\partial r}\right)+\left(\frac{i\omega\mu_0}{ia+\alpha_2 b}\right)\phi_2=0. \tag{18b}$$

We now observe that the quantity in the right parentheses may be considered as the square of a transverse wave number T, so we have

$$T^2=\omega\mu_0/(a-i\alpha b) \tag{19}$$

and we write the quadratic equation implied above in terms of T^2 instead of α with the result

$$(\gamma_1^2-\gamma_2^2)\left[\gamma_1^2-\gamma_2^2+\gamma_1T^2+\frac{\epsilon_1T^2}{\epsilon_3}\left(\gamma_1+\frac{\gamma_2\epsilon_2}{\epsilon_1}+T^2\right)\right]=0. \tag{20}$$

The solution $\gamma_1^2-\gamma_2^2=0$ corresponds to the trivial solution $\phi_0=0$, and we will not consider it further. The other factor yields the dispersion relation for the hydromagnetic waves, although T^2 must be determined from Eq. (20) along with the boundary conditions. We note that Eq. (20) is quadratic in T^2 so that there are two values of T^2 for each value of γ_1.

To construct the solutions of the differential equations we observe that solutions of Eqs. (18a, b), which are regular on the axis, are

$$\phi_1(r)=AJ_0(T_1r), \tag{21a}$$

$$\phi_2(r)=\tau AJ_0(T_2r). \tag{21b}$$

We now use these to construct the axial field expressions

$$H_z(r,z,t)=A[J_0(T_1r)+\tau J_0(T_2r)]e^{i(\omega t-kz)}, \tag{22a}$$

$$E_z(r,z,t)=A[\alpha_1J_0(T_1r)+\alpha_2\tau J_0(T_2r)]e^{i(\omega t-kz)}, \tag{22b}$$

where τ is determined by the boundary condition and A is an excitation coefficient. Using Eqs. (22a, b) the expressions for the other field components may be derived.

If we now consider the plasma to be contained in a cylindrical conducting waveguide of radius a so that the tangential electric fields vanish at the wall, the boundary condition $E_z(a)=0$ leads to

$$\left(\gamma_1+\frac{\gamma_2\epsilon_2}{\epsilon_1}+T_1^2\right)J_0(T_1a)+\tau\left(\gamma_1+\frac{\gamma_2\epsilon_2}{\epsilon_1}+T_2^2\right)J_0(T_2a)=0, \tag{23}$$

and it may be shown that the boundary condition $E_\theta(a)=0$ leads to

$$J_1(T_1a)/T_1+\tau J_1(T_2a)/T_2=0. \tag{24}$$

Eliminating τ from the above equations we obtain

$$\left(\gamma_1+\frac{\gamma_2\epsilon_2}{\epsilon_1}+T_1^2\right)T_1J_0(T_1a)J_1(T_2a)=\left(\gamma_1+\frac{\gamma_2\epsilon_2}{\epsilon_1}+T_2^2\right)T_2J_0(T_2a)J_1(T_1a), \tag{25}$$

[12] A. G. Lieberman, Ph.D. Thesis, California Institute of Technology (1964).

which, along with Eq. (20), completely determines a set of values for T_1, T_2, and k, and the set characterizes a single mode for a given frequency and set of plasma conditions. In general, there exists an infinite set of modes which satisfies Eqs. (20) and (25) and, in fact, we can distinguish two distinct classes of modes, each of which contains an infinite number of modes. In the magnetohydrodynamic limit ($\omega \ll \Omega_c$) one of these classes, which we call the compressional modes, may be identified with the TE modes of Newcomb,[5] while the other class of modes, which we call the torsional modes (and designate with primes), may be identified with his Principal modes.

The general steady state solution is then given by a superposition of all these modes so we have for H_z, for example,

$$H_z(r, z, t) = \sum_m A_m[J_0(T_{1m}r) + \tau_m J_0(T_{2m}r)]e^{i(\omega t - k_m z)} + \sum_n A_n'[J_0(T_{1n}'r) + \tau_n' J_0(T_{2n}'r)]e^{i(\omega t - k_n' z)}. \quad (26)$$

IV. LIMITING CASES

The solution of Eqs. (20) and (25) has been obtained with an IBM 7090 digital computer using an iterative procedure. In order to find a starting point for this procedure, we consider $\omega \ll \omega_c < \omega_p$ and neglect damping, in which case it may be shown that ϵ_1/ϵ_3 is of the order of $(\omega/\Omega_c)^2\, m_e/m_i$, which, for frequencies of the order of the ion cyclotron frequency, is of the order of m_e/m_i. If we neglect terms of this order, the dispersion relation becomes

$$\gamma_1^2 - \gamma_2^2 + \gamma_1 T^2 = 0. \quad (27)$$

This expression is not quadratic in T^2, so there is only one value of T for each mode. Equation (26) also yields $\alpha = 0$, so $E_z = 0$, and now the boundary condition yields from $E_\theta(a) = 0$ that $J_1(T_m a) = 0$ for both classes of modes, so that the T_m are given by $Ta = 3.83$, 7.01, etc. It may be shown that τ_m in Eq. (26) approaches zero as ϵ_1/ϵ_3 approaches zero, so the term involving T_2 drops out of the field expressions. The dispersion relation for the two classes of modes is now given from Eq. (27) by

$$k_m^2 = \omega^2\mu_0\epsilon_1 - \tfrac{1}{2}T_m^2 \pm [(\tfrac{1}{2}T_m^2)^2 + (\omega^2\mu_0\epsilon_2)^2]^{\frac{1}{2}} \quad (28)$$

where the upper sign is associated with the torsional modes.

It may be shown, on the other hand, that at very low frequencies $\omega \ll \Omega_c \ll \nu_{ei}$ an appropriate approximation is to neglect ϵ_2. This approximation decouples the differential equations (18a, b) so H_θ and E_r may be expressed in terms of E_z while H_r and E_θ may be expressed in terms of H_z, and now there are separate differential equations for E_z and H_z.

The modes which have the axial electric field may be identified with the torsional modes above, but now the boundary condition $E_z'(a) = 0$ leads to $J_0(T_m' a) = 0$, so the T_m' values for this mode are different from their values at higher frequencies. This mode is nearly dispersionless at low frequencies, and in terms of the wave magnetic field, it consists of *torsional* waves (since only $H_\theta \neq 0$) hence our designation as torsional modes. All of these modes travel essentially at the Alfvén speed.

The other modes may be identified with those characterized by the lower sign in Eq. (28) above, and the boundary condition leads to $J_1(T_m a) = 0$ again, so the T_m values are unchanged at low frequencies. The dispersion relation for these modes after neglecting terms of order ω/Ω_c is

$$k_m^2 = (\omega^2/V_A^2) - T_m^2, \quad (29)$$

which is analogous to ordinary waveguide propagation except that the characteristic velocity is the Alfvén velocity. These modes exhibit the characteristic waveguide cutoff phenomena, and from equation (29) we find the cutoff frequency to be given by

$$\omega_{0m} = T_m V_A, \quad (30)$$

a result which does not depend on the fact that $\omega \ll \Omega_c$. Since these modes have a component of the wave magnetic field in the direction of the static magnetic field, the static field lines are alternately compressed and expanded, hence we have designated them *compressional modes* and the experiment is restricted to these modes only.

It should be noted that the cutoff phenomena may be thought of as being due to waves which travel in all directions and which reflect from the walls according to the boundary condition. At the cutoff frequency the waves travel only perpendicular to the magnetic field and the wave oscillates in phase down the entire waveguide. The wave which propagates across the field is often called a magnetoacoustic wave, but it is here a special case of compressional wave propagation.

In order to illustrate the exact behavior of the T values, Fig. 2 shows the exact solution for the lowest torsional mode, where the change of $T_1 a$ from 2.405 to 3.832 is apparent, while Fig. 3 shows the deviation of $T_1 a$ from 3.832 for the lowest compressional mode.

V. IMPULSE RESPONSE FOR LOOP EXCITATION

Using orthogonality relations which have been determined by A. G. Lieberman,[12] the excitation coefficient for a coaxial current loop of radius b in a waveguide of radius a (where we have considered A_m only, since it may be shown that A_m' is small for loop excitation) is given by

$$A_m = -I_0 b\, \mathcal{E}_{\theta m}(b)\left\{2\int_0^a (\mathcal{E}_{rm}\mathcal{H}_{\theta m} + \mathcal{E}_{\theta m}\mathcal{H}_{rm}) r\, dr\right\}^{-1}, \tag{31}$$

where the current $I = I_0 e^{i\omega t}$ and the script notation denotes the field expressions without any excitation coefficient. With the excitation coefficient above, the steady state response is the Fourier transform of the response to an impulse, $I = I_0\,\delta(t)$ since the transform of I is I_0. Therefore the impulse response of the system is given by the inverse Fourier transform of the steady state response, or

$$H_z(r, z, t) = \sum_m \int_{-\infty}^{\infty} A_m(\omega)[J_0(T_{1m}r) + \tau_m J_0(T_{2m}r)]e^{i(\omega t - k_m z)}\frac{d\omega}{2\pi}. \tag{32}$$

For the response to an arbitrary driving current we simply replace I_0 in (31) by the Fourier transform of the current $I(\omega)$.

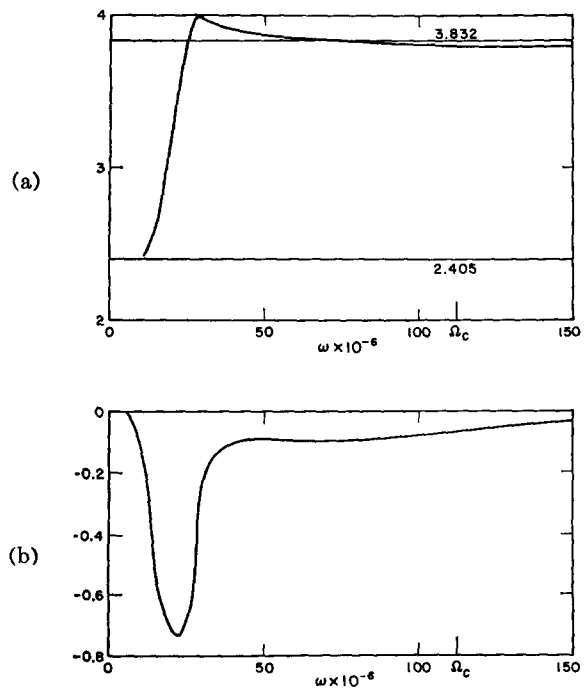

FIG. 2. (a) Re $(T_1'a)$ vs ω for lowest torsional mode. (b) Im $(T_1'a)$ vs ω for lowest torsional mode. ($B_0 = 1.17\text{W/m}^2$, $n = n_0 = 6.61 \times 10^{21}\ \text{m}^{-3}$, $\eta = 5 \times 10^{-4}\ \Omega\,\text{m}$, $a = 6.75$ cm).

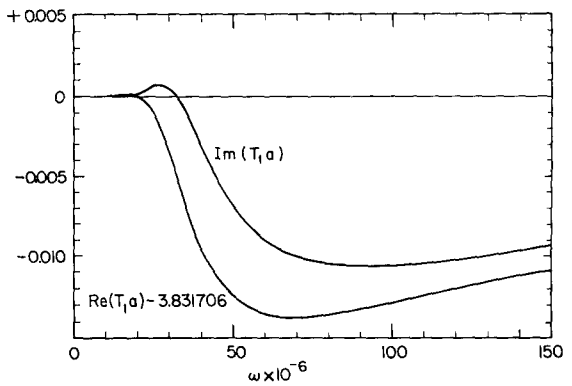

FIG. 3. T_1a vs ω for lowest compressional mode. (Same parameters as Fig. 2 except $n = 0.7n_0$ and $\nu = 1.65 \times 10^7$ radians/sec).

VI. APPARATUS AND PLASMA PREPARATION

The basic geometry of the apparatus is similar to that of Wilcox, *et al.*,[2] and a schematic diagram is shown in Fig. 1. The waveguide and electrode were 304 stainless steel and the end plates were pyrex. Alumina probe sheaths and a pyrex encased circular loop were used. The magnetic field was pulsed, the current rising to its maximum in about 0.7 msec, so the field was within 1% of its maximum value for over 100 μsec. A lumped constant delay line produced a 1.5×10^4 A, 10–15 μsec discharge between the electrode and the tube wall which drove an ionizing wave[13] along the tube at about 5 cm/μsec. The background pressure in the vacuum system was about 2×10^{-6} Torr, to which a static atmosphere of hydrogen in the range 0.02–0.25 Torr was admitted just before the plasma preparation.

The plasma which is formed by the ionizing wave is known to be somewhat turbulent and nonuniform, having a core which is cooler than the annular region. The radial and longitudinal diffusion times should be 100 μsec or greater so that the plasma is quite steady during the wave experiment, which never lasts more than 2 μsec.

The wave is excited by a coaxial loop with a critically damped RLC circuit supplying a current pulse about 40 nsec in duration. The loop radius was chosen so as to minimize the excitation of the second circularly symmetric mode, but all other modes are excited.

The signals were detected by 10-turn magnetic probes and were passed through high pass filters before entering the dual beam oscilloscope to eliminate pickup from the slowly changing magnetic

[13] W. B. Kunkel and R. A. Gross, "Hydromagnetic Ionizing Waves," Lawrence Radiation Laboratory Report UCRL 9612 (1961).

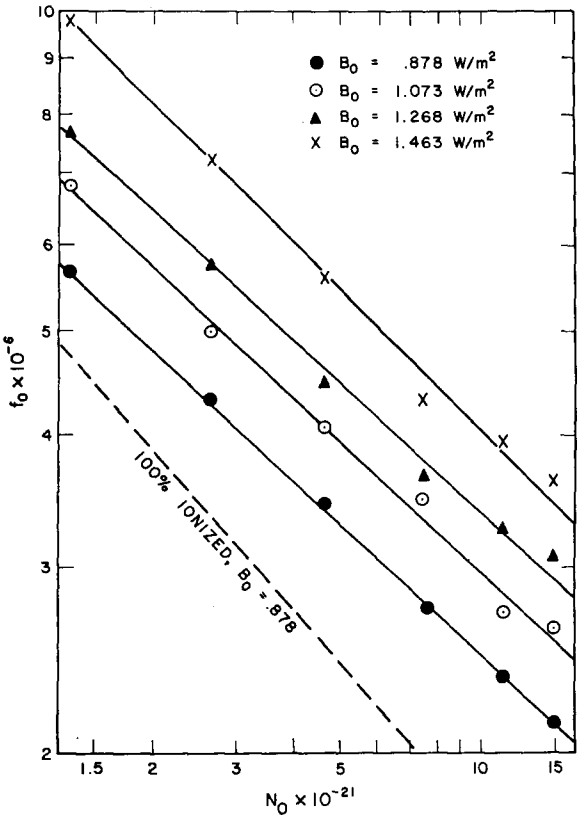

FIG. 4. Cutoff frequency vs initial particle density.

field. The system response was essentially constant between 1 and 20 Mc/sec.

VII. EXPERIMENTAL RESULTS—CUTOFF FREQUENCY ANALYSIS

For the compressional mode the lowest frequency at which the wave will propagate is the cutoff frequency ω_0, given by Eq. (30), and the group velocity approaches zero near this frequency. The group velocity for higher frequencies is always higher, so the last frequency to appear at the magnetic probe due to an impulse excitation is the cutoff frequency. This frequency can easily be measured approximately from the photographs of the received signals, and since it is proportional to the Alfvén speed, we can study the dependence of this quantity upon magnetic field and density. Measuring the cutoff frequency in this manner introduces a small systematic error, because the damping prevents the measurement from being made at very late times, but this error is usually small and always results in a measured frequency, which is slightly higher than the actual frequency. For each of more than 125 pictures, the last observable frequency was measured, generally by taking an average of the last three or four half cycles.

The results of this parameter study are shown in Figs. 4 and 5. Figure 4 shows the dependence of ω_0 upon the initial density for several values of the magnetic field. N_0 here represents the assumed total particle density including ions and atoms and is deduced from the gauge pressure before the discharge. Since the ionizing wave may drive some of the original gas to the end of the tube, this may introduce a systematic error in our estimate of the degree of ionization and of the ion–neutral collision frequency. Each point represents an average taken from two or three pictures. For the lowest magnetic field (B = 0.878 W/m^2) only, a 100% ionization reference line is indicated for comparison purposes.

From the data of Fig. 4 we can estimate the maximum impurity ion mass density as follows. If the amount of hydrogen were progressively decreased, the Alfvén speed, and hence the cutoff frequency, would be determined ultimately by the impurity ion mass density, and a limiting cutoff frequency would appear. From the highest values of ω_0 in Fig. 4 and the fact that no limiting is apparent, we estimate that the ion mass density of the impurities is less than the ion mass density of hydrogen at $n = 3 \times 10^{20}$ m^{-3}.

We also note that the observed cutoff frequencies are all above the values which would correspond to 100% ionization, which we interpret as meaning that the plasma is not fully ionized. In fact, with this interpretation, the data of Fig. 4 indicates that the percent ionization varies smoothly from about 75% ± 5% at the lowest initial densities to 45% ± 3% at the highest densities indicated.

With the same interpretation, the data of Fig. 5 may be taken to indicate that there is no systematic variation of the degree of ionization with magnetic field. If there were some systematic variation of the degree of ionization with magnetic field, one would

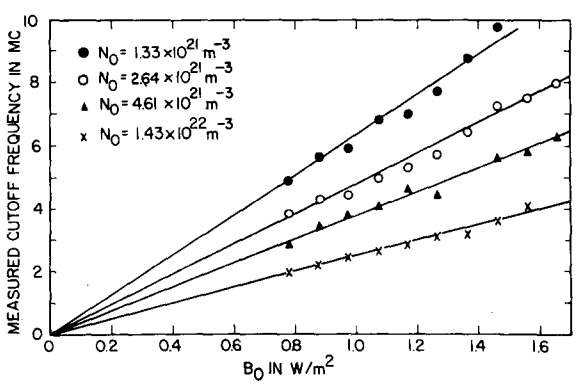

FIG. 5. Cutoff frequency vs magnetic field strength.

expect a straight line through the origin to be a poor fit to the data. However, a least squares analysis of the data shown, along with other data at different densities, indicates that the lines do extrapolate very closely to the origin. Hence, we find no evidence of a systematic variation of the percentage ionization with the magnetic field.

VIII. EXPERIMENTAL RESULTS—TRANSFER FUNCTION ANALYSIS

The most critical test of the adequacy of the plasma model involves the study of the dispersion relation for the compressional wave over the entire range of frequencies from below cutoff up to the vicinity of the ion cyclotron frequency. Since the plasma conditions are not highly reproducible from shot to shot, we have obtained the transfer function of the plasma for single shots by Fourier analysis of the impulse response. We define the transfer function $G(\omega, z)$ as the ratio of the Fourier transform of the axial magnetic field at $r = 0$ to the transform of the loop current

$$G(\omega, z) \equiv e^{-ik'z} \equiv \mathfrak{F}[H_z(0, z, t)]/I(\omega). \qquad (33)$$

From Eq. (32), $G(\omega, z)$ is given by

$$G(\omega, z) = \frac{1}{I(\omega)} \sum_{\mathrm{m}} A_{\mathrm{m}}(1 + \tau_{\mathrm{m}})e^{-ik_{\mathrm{m}}z}. \qquad (34)$$

In the analysis of the data the values of $k' = \beta' - i\alpha'$ are evaluated on an IBM 7090 digital computer from oscillograms of the received and driving signals and compared with theoretical values computed from Eq. (34). An example of the oscillograms is shown in Fig. 6, where the impulse is shown in the upper trace (retouched because of faintness) for reference and the received signal is shown below.

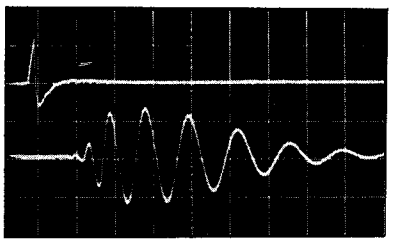

FIG. 6. A typical photograph of a received signal. The upper trace is the time derivative of the driving current as measured with a magnetic probe, and is displayed for timing reference (arbitrary amplitude). The lower waveform is the signal received from a magnetic probe which measures the time derivative of the axial component of the wave magnetic field on axis, 20 cm from the driving loop. The vertical sensitivity for the lower waveform is 20 G/μsec/div. The horizontal scale is 0.2 μsec/div.

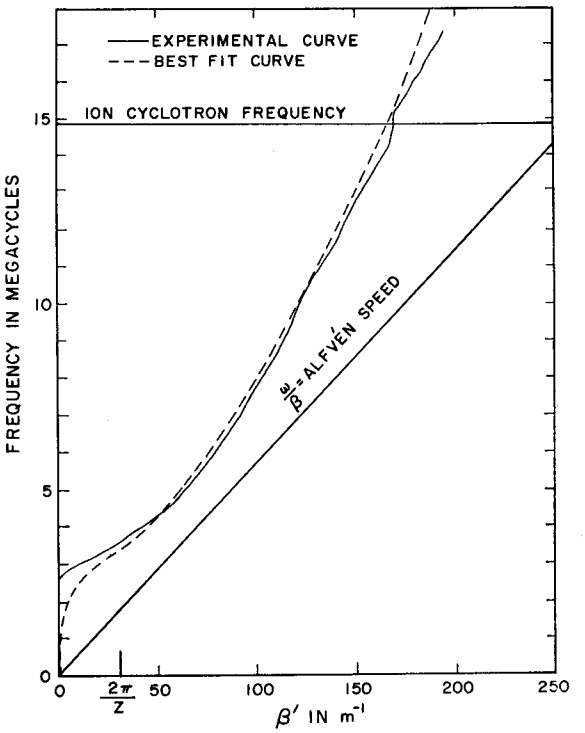

FIG. 7. Frequency vs transfer function effective propagation constant at $z = 0.2032$ m.

Over twenty such pictures covering a variety of magnetic fields and initial densities have been analyzed in detail.

The transfer function (phase and amplitude) of the signal shown in Fig. 6, computed as described above, is shown in Figs. 7 and 8 as an example of the type of information which may be extracted from such an oscillogram. Also included in Figs. 7 and 8 are the "best fit" theoretical transfer function phase and amplitude curves which were determined by a curve fitting procedure described below.

In the curve fitting procedure, the values of the magnetic field (calibrated to 2%), the initial density (McLeod gauge calibrated), and the dimensions of the system were assumed to be known exactly, but the resistivity η, the ion–neutral collision frequency ν, and the percent ionization γ were treated as disposable parameters. The three disposable parameters were selected so as to minimize a weighted average error, computed from the differences between theoretical and experimental curves at about ten frequencies and weighted according to our estimates of the probable errors in the experimental curves at those points. The location of the minimum was determined to a few percent, but this does not at all guarantee the best fit values are accurate to that tolerance.

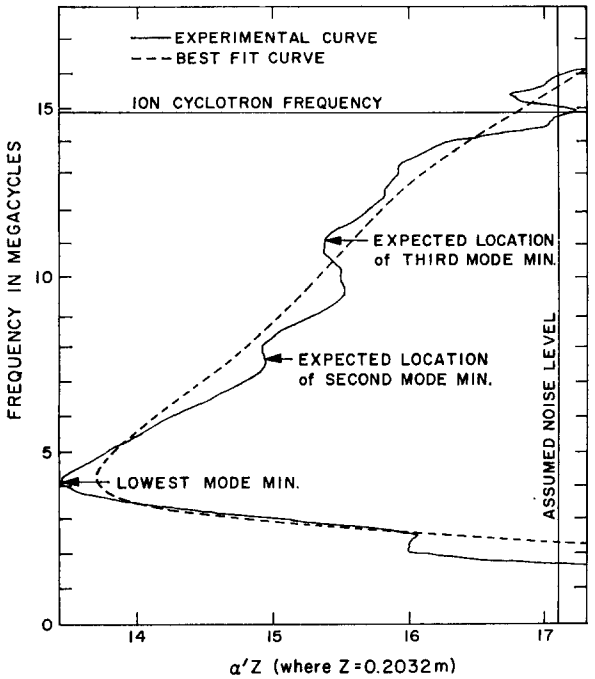

FIG. 8. Frequency vs transfer function effective attenuation constant.

Several characteristic features of the experimental transfer functions are apparent in the example shown. We observe that the shape of the phase curve generally fits the theoretical curve very well except near and below cutoff and at high frequencies where the amplitude is very small. In many cases the fit was even better than in the example shown.

It is apparent that the experimental and theoretical amplitude curves do not fit quite as well as the phase curves, although the general features match well. Since the resistivity and the ion–neutral collision frequency are primarily determined from the amplitude curve, we may expect the errors to be somewhat larger in the determination of these quantities than for the degree of ionization which is primarily determined from the phase curve. One feature of the experimental amplitude curves is that there appears to be more evidence of higher modes than in the theoretical amplitude curves. We note that evidence of the second mode appears even though we designed the excitation loop to excite none of that mode. This may be due to the radial nonuniformity of the plasma, which can be expected to affect the excitation coefficients more than the propagation characteristics.

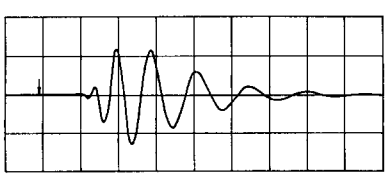

FIG. 9. Time waveform derived theoretically from "best fit" parameters (compare with Fig. 6). The horizontal and vertical scales have been adjusted to agree with Fig. 6, and the arrow denotes the start of the pulse.

There is some evidence that the values obtained for ν and/or η are too high. If the inverse Fourier transform of the best fit transfer function is taken to produce a time function, the amplitude of the theoretical signal is systematically lower than that of the experimental signal, and the envelope indicates a higher damping rate. The time function derived from the best fit curves of Figs. 7 and 8 is shown in Fig. 9 where these features may be seen from comparison with Fig. 6. It appears that if the curve fitting had been done in the time domain instead of the frequency domain, somewhat smaller values might have been obtained for η and ν. Since the phase agreement is quite satisfactory we expect the determination of the degree of ionization to be good.

Even though there may be some systematic errors in the determination of η and ν, we expect that trends should be apparent. The only one which was clearly observed was that the resistivity appeared to increase with the magnetic field. This trend is shown in Fig. 10 where the error bars are intended to show our estimate of the relative probable errors and indicate the range over which η must be varied to double the weighted average error. A possible explanation of the variation of the resistivity with magnetic field is offered below.

In general the degree of ionization determinations showed the least uncertainties. Typically a 5% change in γ would double the weighted average error. The value of γ determined by curve fitting was 6% ± 12% higher than that computed from the

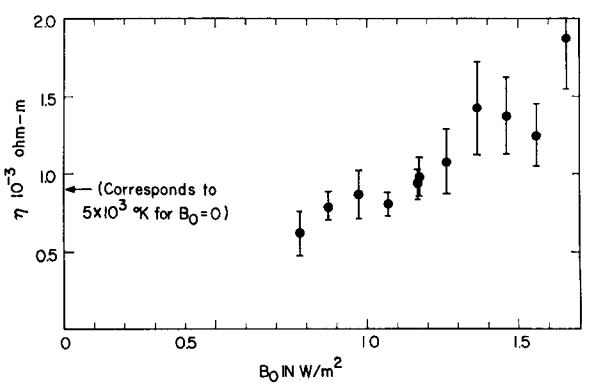

FIG. 10. "Best fit" value of resistivity vs magnetic field strength.

measured cutoff frequency so both methods are believed to be consistent and give rather good estimates of the average ion density, although no independent measurements have been made.

There was considerable scatter in the value of the ion–neutral collision frequency determined from curve fitting, and the uncertainties indicated a variation of ν by a factor of two would only double the weighted average error. No systematic trends were apparent, so we simply averaged the quantity $\langle \sigma v_n \rangle$ where σ is the ion–neutral cross section and v_n is the neutral thermal speed, and we have assumed

$$\nu = \gamma n_0 \langle \sigma v_n \rangle. \tag{35}$$

The result is that $\langle \sigma v_n \rangle = (5.5 \pm 1.3) \times 10^{-15}\ \mathrm{m^3/sec}$.

We have made measurements of the radial dependence of the axial component of the wave magnetic field and found fairly good agreement with the theoretical profile as is shown in Fig. 11. The experimental profile supports our assumptions about the boundary condition, although some other assumption might lead to a similar profile.

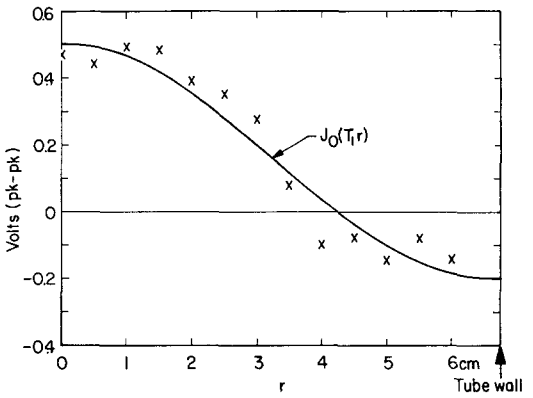

FIG. 11. Radial amplitude variation.

IX. CONCLUSIONS

It is felt that the general agreement between theoretical and experimental phase curves indicates that the theory adequately describes the dispersion characteristics of the compressional waves in a waveguide. From this type of data the average degree of ionization can probably be determined within 5%, and from the cutoff frequency the error may be about 10%. A possible inadequacy of the theory is the variation of the resistivity with magnetic field, illustrated in Fig. 11. This effect may be due to some systematic error in the experiment of which we are not aware, or it may be due to a systematic change in the temperature with magnetic field. Both these possibilities seem unlikely, although no independent temperature measurements have been made.

We believe the trend may be due to an inadequacy of the theory, which assumes η to be a scalar quantity, whereas if ω_c/ν_{ei} is of the order of unity or greater, the resistivity is a tensor.[14] Now ω_c/ν_{ei} is of the order of unity for the data of Fig. 10, and since the compressional wave is primarily dependent on the transverse resistivity, we may have simply observed the onset of the tensor character of η. While all the data of Fig. 10 is at a constant density, we are presently trying to extend the range of the parameter ω_c/ν_{ei} by studying other ion densities to see if η becomes independent of ω_c/ν_{ei} at extreme values of this parameter as would be expected if this were the proper explanation of the effect.

ACKNOWLEDGMENTS

This work was supported by the U. S. Air Force Office of Scientific Research under Grant No. 412-63.

[14] W. Marshall, "Kinetic Theory of an Ionized Gas", Pt. 3, U. K. Atomic Energy Research Establishment T/R 2419 (1960).